International Journal of Heat and Mass Transfer 51 (2008) 5209–5225

Contents lists available at ScienceDirect

International Journal of Heat and Mass Transfer

journal homepage: www.elsevier.com/locate/ijhmt

The heat/mass transfer analogy for a simulated turbine blade

S. Han, R.J. Goldstein *

Department of Mechanical Engineering, Heat Transfer Laboratory, University of Minnesota, 1200 Mechanical Engineering Building, 111 Church Street S.E., Minneapolis, MN 55455, USA

ARTICLE INFO

Article history:
Received 19 September 2007
Received in revised form 9 February 2008
Available online 2 June 2008

Keywords:
The heat/mass transfer analogy
Naphthalene sublimation
Thermal boundary layer
Constant temperature
Constant concentration
Gas turbine
Turbine blade

ABSTRACT

Due to the complexity of the flow and the difficulty of measuring heat transfer directly in gas turbines or even in turbine cascade, heat transfer coefficients have been extracted from data obtained in mass transfer measurements using the heat/mass transfer analogy.
The present paper shows the validity of the heat/mass transfer analogy from separate heat transfer and mass transfer measurements on simulated turbine blades with equivalent experimental and geometric conditions. The Nusselt numbers from heat transfer experiments employing a constant temperature boundary condition are compared to the Sherwood number from mass transfer experiments employing a constant concentration boundary condition.

1. Introduction

Mass transfer experiments have been extensively used to determine heat transfer coefficients using the heat/mass transfer analogy. Local mass transfer results can be obtained under laboratory conditions with a high resolution in a short time period. Mass transfer experiments are free from conduction and radiation errors which are inherent in heat transfer studies. However, when heat transfer results are required in complex flows, detailed local heat/mass transfer analogy factors may be required to convert the mass transfer data into heat transfer results.

The heat/mass transfer analogy is derived from the conservation equations of momentum, energy and concentration of a constant property fluid by Nusselt [1] and Schmidt [2]. The heat/mass transfer analogy implies that heat transfer results can be converted from the mass transfer data under equivalent experimental conditions and vice-versa. This follows from the similarity of the equations governing heat and mass transfer.

The non-dimensional heat transfer equation

$$\frac{D\theta}{D\tau} = \frac{1}{RePr}\frac{\partial}{\partial \hat{x}_i}\left(\left(1+\frac{\epsilon}{\nu}\frac{Pr}{Pr_t}\right)\frac{\partial\theta}{\partial \hat{x}_i}\right) \quad (1)$$

and the non-dimensional mass transfer equation

$$\frac{Dm}{D\tau} = \frac{1}{ReSc}\frac{\partial}{\partial \hat{x}_i}\left(\left(1+\frac{\epsilon}{\nu}\frac{Sc}{Sc_t}\right)\frac{\partial m}{\partial \hat{x}_i}\right) \quad (2)$$

are very similar. Hence, if the boundary conditions are equivalent for a given geometry, if Pr is equal to Sc, and Pr_t is equal to Sc_t, then 'θ' in Eq. (1) and 'm' in Eq. (2) have the same variations. This essentially describes the heat/mass transfer analogy.

It should, however, be noted that the Prandtl number in a heat transfer experiment is typically different from the Schmidt number in a mass transfer experiment. Therefore, the usefulness of the heat/mass transfer analogy requires simple relations for the case of unequal Prandtl and Schmidt numbers.

Lewis [3] showed that the heat and mass transfer coefficients can be accurately related using an expression from universal velocity profiles in a turbulent boundary layer. Chen and Goldstein [4] used $n = 1/3$ to get an analogy factor with the Colburn relation $\frac{Nu}{Sh} = \left(\frac{Pr}{Sc}\right)^n$. Goldstein and Cho [5] reviewed the naphthalene sublimation technique and the heat/mass transfer analogy with a constant heat flux boundary condition. They recommended $n = 1/3$ for a laminar flow and $n = 0.14$ for wake regions in a Colburn type relation. Eckert et al. [6] compared experimental data with the heat/mass transfer analogy for laminar, turbulent, and three-dimensional flow. However, comparison across different studies is difficult due to the different geometric and experimental conditions. Yoo et al. [7] measured local and average mass transfer rates from a rectangular cylinder. They compared the mass transfer results with heat transfer results from a constant heat flux experiment. It was concluded that the discrepancy between heat and mass transfer results comes from the difference in the boundary condition, the effect of 'n' in the Colburn relation, conduction error in heat transfer and mechanical erosion in mass transfer. Apparently, no heat and

* Corresponding author. Tel.: +1 612 625 5552.
E-mail address: rjg@me.umn.edu (R.J. Goldstein).

0017-9310/$ - see front matter © 2008 Elsevier Ltd. All rights reserved.
doi:10.1016/j.ijheatmasstransfer.2008.04.002

Nomenclature

AR	inlet/exit area ratio of the cascade, =2.72
C_l (C_L)	chord length, $C_l = 184$ mm in present study
C_x	axial chord length of blade, =130 mm in present study
D_{naph}	mass diffusion coefficient
F	local analogy factor, $F = Nu/Sh$
H	height of blade, =457 mm
h	heat transfer coefficient
h_m	mass transfer coefficient
m	dimensionless mass fraction
M_{naph}	molecular mass for naphthalene, $M_{naph} = 129.17$ kg/kmol
n	power index used in heat/mass transfer analogy
n	the distance in the direction normal to the wall
Nu	Nusselt number, $Nu = h \cdot C_l/k$
P	pitch of blade, =138 mm
$p_{v,w}$	naphthalene vapor pressure at the wall
Pr	Prandtl number, $Pr = \nu/\alpha$
Pr_t	turbulent Prandtl number, $Pr_t = \epsilon/\epsilon_H$
q_w	heat flux from the wall
R	gas constant for naphthalene ($C_{10}H_8$), $R = 0.06487$ J/g K
$\overline{R}$	Universal gas constant
Re_{ex}	exit Reynolds number, $= \rho U_{ex} C_l/\mu$
S	curvilinear coordinate on the blade
S_p	curvilinear coordinate on the pressure surface, cf. Fig. 2
S_s	curvilinear coordinate on the suction surface, cf. Fig. 2
Sc	Schmidt number, $Sc = \nu/D_{naph}$
Sc_t	turbulent Schmidt number, $Sc_t = \epsilon/\epsilon_M$
Sh	Sherwood number, $Sh = h_m \cdot C_l/D_{naph}$
St	Stanton number, $St = \frac{Nu}{RePr} = h/\rho c_p U_\infty$
St_m	mass transfer Stanton number, $St_m = \frac{Sh}{ReSc} = h_m/U_\infty$
T_w	wall temperature
T_∞	free stream temperature
T_{aw}	adiabatic wall temperature
$T_{n,w}$	surface temperature of naphthalene
Tu	turbulence intensity, $Tu = \frac{\sqrt{\overline{u'^2}}}{U_\infty}$
U_∞	mainstream inflow velocity in wind tunnel
x	coordinate in blade chord direction
x_i	coordinate along the inflow direction, cf. Fig. 2
y	coordinate traverse to the blade chord direction
Z	coordinate in spanwise direction of cascade, $Z = 0$ at the top

Greek symbols

$\delta\tau$	time duration of data run
δt	sublimation depth of naphthalene
ϵ	turbulent momentum diffusivity
ϵ_H	turbulent thermal diffusivity
ϵ_M	turbulent mass diffusivity
ρ_s	density of solid naphthalene
$\rho_{v,\infty}$	naphthalene vapor density in free stream
$\rho_{v,w}$	naphthalene vapor density at the surface
θ	dimensionless temperature difference
k	thermal conductivity of air

Superscript

^	non-dimensional parameter

Subscripts

atm	atmosphere property
st	static property
w	wall property

mass transfer comparisons have been performed with equivalent boundary conditions on the same geometry for the evaluation of the analogy. With a turbulent boundary layer, the effect of different thermal boundary conditions may not be as important as in a laminar flow. However, a constant wall heat flux condition is not equivalent to a constant wall concentration condition and generally results in a different heat transfer coefficient. Therefore, a constant wall temperature boundary condition is required to get accurate heat/mass transfer analogy factors when a comparison is to be made with a mass transfer study, with a constant wall concentration boundary condition.

The present paper investigates the validity of the analogy and determines the analogy factor with equivalent boundary conditions on a simulated turbine blade through heat and mass transfer experiments. For the mass transfer experiment, the naphthalene sublimation technique is employed to obtain local mass transfer coefficients. For the heat transfer experiment, a thermal boundary layer measurement technique is used to obtain local heat transfer coefficients while maintaining the wall at constant temperature.

In a companion paper [8], the heat/mass transfer analogy on a endwall is investigated with similar heat and mass transfer experimental techniques.

2. Extended heat/mass transfer analogy

Eckert et al. [6] indicated three methods of applying the extended heat/mass transfer analogy. One is deduced from the Navier–Stokes equation for a constant property fluid. Another is obtained from empirical expressions of heat and mass transfer equations for a specified flow. The third involves the assumption that local Nusselt numbers are proportional to the local Sherwood numbers with the averaged analogy factor ($\overline{Nu}/\overline{Sh}$).

The Nusselt (Nu) and Sherwood (Sh) numbers are a function of the Prandtl and Schmidt numbers, respectively, in addition to the Reynolds number and the geometry. Their local values can be described as

$$Nu = f(Re, Pr, \hat{x}_i), \quad Sh = f(Re, Sc, \hat{x}_i) \tag{3}$$

For laminar flow on a flat plate, the relations in Eq. (4) are used to obtain Nusselt and Sherwood numbers

$$Nu = C_1 Re^m Pr^n, \quad Sh = C_1 Re^m Sc^n \tag{4}$$

However, the Prandtl number of air in the region studied is ≈0.7 while the Schmidt number of naphthalene (in air) is ≈2.28. This means that an analogy factor is required to obtain Nu from Sh and vice-versa

$$Nu = F \cdot Sh \tag{5}$$

Thus, for the same Reynolds number, the analogy factor for a flat plate can be expressed as

$$F = \frac{Nu}{Sh} = \left(\frac{Pr}{Sc}\right)^n \tag{6}$$

where the exponent 'n' is determined from known solutions. For a laminar flow, $n = 1/3$ is obtained from the solution of the Blasius equations resulting in $F = 0.677$ for $Pr = 0.707$ and $Sc = 2.28$.

For turbulent flow on a flat plate, a Stanton number correlation was developed by Eckert and Drake [9]

$$St = \frac{0.0296 Re_x^{-1/6}}{1 + 1.48 Re_x^{-1/10} Pr^{-1/6}(Pr - 1)} \tag{7}$$

An analogy factor equation can be obtained from Eqs. (3) and (7)

$$F = \left(\frac{Pr}{Sc}\right) \frac{1 + 1.48 Re_x^{-1/10} Sc^{-1/6}(Sc - 1)}{1 + 1.48 Re_x^{-1/10} Pr^{-1/6}(Pr - 1)} \tag{8}$$

The analogy relation of Eq. (8) results in $F = 0.388$ for $Re_x = 1 \times 10^6$ with $Pr = 0.707$ and $Sc = 2.28$.

Kays and Crawford [10] developed another Stanton number correlation for turbulent flow on a flat plate

$$St = \frac{0.0287 Re_x^{-0.2}}{0.85 + 0.169 Re_x^{-0.1}(13.2Pr - 8.66)} \tag{9}$$

An analogy factor can be developed from Eqs. (3) and (9)

$$F = \left(\frac{Pr}{Sc}\right) \frac{0.85 + 0.169 Re_x^{-1/10}(13.2Sc - 8.66)}{0.85 + 0.169 Re_x^{-1/10}(13.2Pr - 8.66)} \tag{10}$$

With $Re_x = 1 \times 10^6$, $Pr = 0.707$ and $Sc = 2.28$, the analogy factor F is 0.479. The analogy factors are listed in Table 1 for different Reynolds numbers.

3. Experimental apparatus and measurement procedure

The test section, shown in Fig. 1, is connected to the exit of the contraction region of a blowing-type wind tunnel. The bottom endwall has a large opening where the heat or mass transfer endwall can be placed. The top endwall has one rectangular window for the insertion of the thermal boundary layer probe and visual observation. The profile of a modern high performance turbine blade, modified for experimental flow conditions, is used for the blades in the cascade. The straight section of the tunnel, with a cross-section of 457 mm × 457 mm and a length of 610 mm, has slots for inserting grid turbulence generators. A 1 mm diameter trip-wire is placed near the exit of the contraction section on the bottom endwall (820 mm upstream of the stagnation point of the central blade), to induce a near-fully-developed turbulent

Table 1
Analogy factors (F) for varying Reynolds numbers

No.	Re_x	Eckert and Drake, Eq. (8)	Kays and Crawford, Eq. (10)
1	1×10^5	0.403	0.548
2	5×10^5	0.393	0.498
3	1×10^6	0.388	0.479
4	5×10^6	0.378	0.440
5	1×10^7	0.374	0.326
6	5×10^7	0.363	0.395

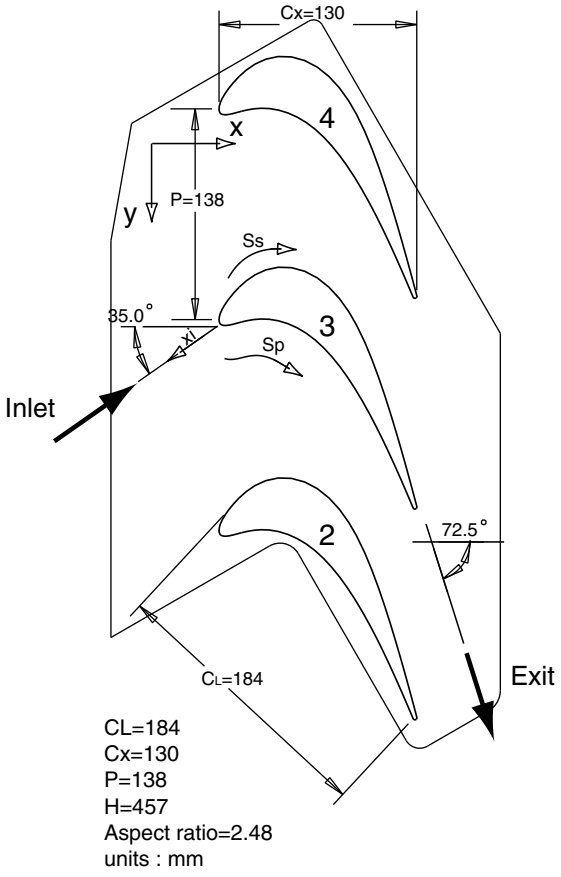

Fig. 2. Blades configuration in the turbine cascade.

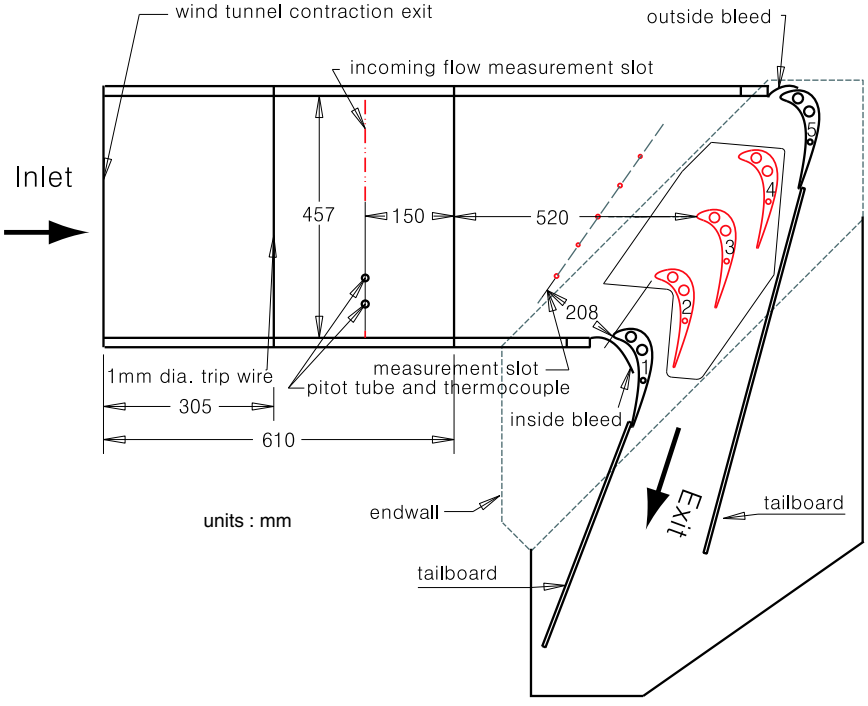

Fig. 1. Test section for the heat and mass transfer experiment.

boundary layer on the endwall at the inlet to the cascade. The cascade exit flow velocity is calculated from the measured incoming flow velocity and the area aspect ratio (2.72).

3.1. Heat transfer experiment

Local heat transfer coefficients are determined from measurements on a constant temperature blade with a thermal boundary layer probe. To increase measurement repeatability and reduce error, a fully automated temperature measurement system was developed at the Heat Transfer Laboratory, University of Minnesota. A detailed description of the heat transfer experiment can be found in Han and Goldstein [11].

3.1.1. Thermal boundary measurement method

Very near the wall, any turbulence fluctuations are small and go to zero at the wall, as does the fluid velocity. The thermal energy is assumed to be transported only by molecular heat conduction in the viscous sublayer region, resulting in a linear temperature variation with distance from the wall. The heat flux can then be evaluated from the thermal gradient as

$$q_w = -k\frac{\partial T}{\partial n} \tag{11}$$

where n is normal to the surface. The heat transfer coefficient is obtained from the heat flux, wall temperature and free stream temperature

$$h = \frac{q_w}{T_w - T_\infty} = \frac{-k\partial T/\partial n}{T_w - T_\infty} \tag{12}$$

From Eq. (12), the local Nusselt number is expressed as

$$Nu = \frac{hC_l}{k} = \frac{-C_l\partial T/\partial n}{T_w - T_\infty} \tag{13}$$

Thus, from Eqs. (12) and (13), the precise evaluation of the heat transfer coefficients and Nusselt numbers depend on the accurate measurement of the temperature in the viscous sublayer region, as well as the free stream and wall temperatures. For this calculation, the wall temperature is obtained by extrapolating the temperatures in the sublayer region. Therefore, one must determine the wall location accurately. The uncertainty in the gradient depends on the boundary layer thickness and fluctuation of the flow. The uncertainty in k is negligible. Therefore, the uncertainty of heat flux is primarily the uncertainty of the temperature measurement. The uncertainties of the heat flux are 8.7% near the leading edge and 4.0% at $S_p/C_l = 0.743$. Thinner boundary layer induces higher conduction error in determining temperature gradients.

3.1.2. Thermal boundary layer probe

A direct temperature measurement with a micro-thermocouple is used to determine the thermal gradient near the wall. The presence of a probe can disturb the flow and influence the heat transfer measurement. High heat transfer regions can generate large thermal gradients near the wall and cause significant conduction errors in a thermocouple probe. Also, a high velocity incoming flow can vibrate the probe. Therefore, the special thermal probe is designed to reduce flow disturbance, to minimize the conduction error and to ensure accurate measurement location.

Blackwell and Moffat [12] reviewed temperature measurements using thermocouple probes. They evaluated the performance of various thermocouples for conduction errors and suggested a butt-welded E-type model. For the present study, the junction of the 76 μm diameter E-type thermocouple is butt-welded by an electric discharge welding technique. The thermocouple probes are shown in Fig. 3. Separate probes are designed for the suction- and pressure-side measurements. The thermocouple junction is supported by two hypodermic needles and located centrally between the needles. A Teflon bar connects two hypodermic needles to maintain the geometry. The suction-side probe is bent clockwise direction when viewed from the top and the diameter of the bent-part is 30 mm. The thermocouple exposure is 14 mm wide and 1 mm high. The pressure-side probe is bent counterclockwise direction when viewed from the top and the diameter of the bent-part is 25 mm. The probes have different diameters to ease measurements on the suction and pressure surfaces.

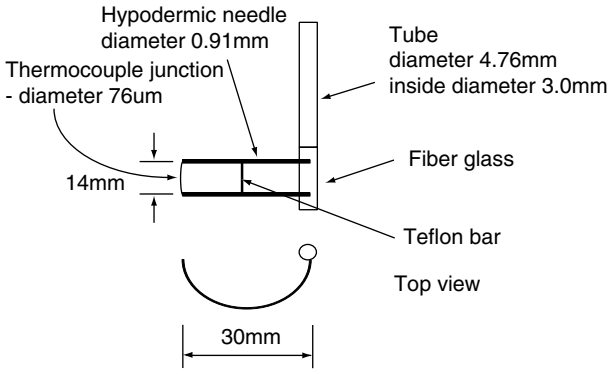

(a) for suction wall measurement

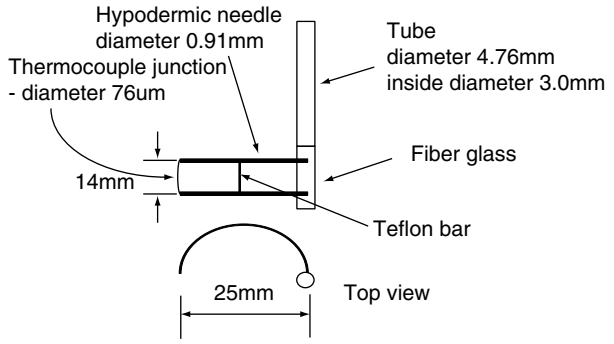

(b) for pressure wall measurement

Fig. 3. Thermal boundary layer probe schematic.

3.1.3. Five-axis measurement unit

To determine the heat flux from the temperature gradient near the wall, temperatures should be measured in a direction normal to the wall with high accuracy. As mentioned previously, it is also critical to know the location of the wall to determine its temperature. The uncertainty in the measurement of the positions of the probe and the wall should be small to compare heat and mass transfer results at the same location on the blade. To achieve this purpose, a five-axis measurement unit has been designed to locate the probe at specified positions and to measure temperatures above and perpendicular to the wall. The wall position is monitored by a programmable limit switch in a motion controller. It consists of four unislides ('x', 'y', 'z', and 'n'), one rotating table ('θ' in Fig. 4), a supporter and a modified five-axis motion controller. The thermal boundary layer thickness is generally about 500 μm for $Re_{ex} = 2 \times 10^5$. The measurement system has a resolution of 5 μm, two orders of magnitude smaller than the thickness of the thermal boundary layer. The five-axis system is connected to a supporter to reduce vibrations from the wind tunnel. The probe is attached to the z-axis slide and connected to an electrical circuit to find the wall position. When the probe touches the wall, it closes the electrical circuit and recognizes the wall position. Since the res-

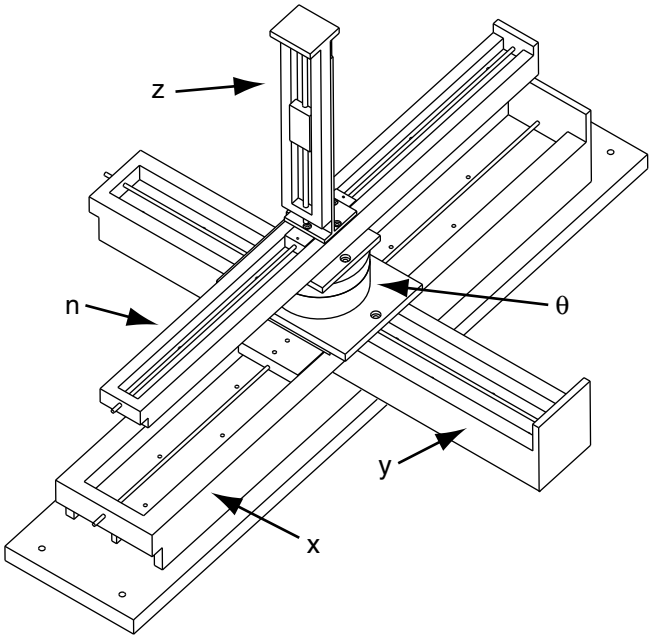

Fig. 4. Five-axis measurement unit sketch.

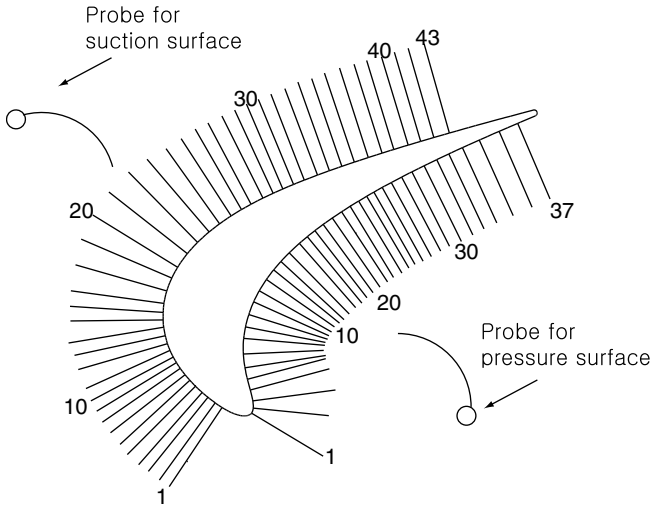

Fig. 5. Blade measurement positions for heat transfer experiments.

olution of the unislide is 5 μm, the wall position is located with position error in the range of ±2.5 μm. For the heat transfer measurements, 43 positions along the suction surface and 37 positions along the pressure surface are selected (cf. Fig. 5). The straight lines in Fig. 5 represent the probe positions when moved normal to the blade surfaces.

3.1.4. Heat transfer blade and temperature control unit

The complicated secondary flows (cf. Fig. 6) in a turbine cascade induce large thermal gradients over the turbine endwall and blade. Therefore, a major challenge in this heat transfer experiment is to maintain a constant wall temperature boundary condition. The blade active (heated) portion was designed, based on a simulation

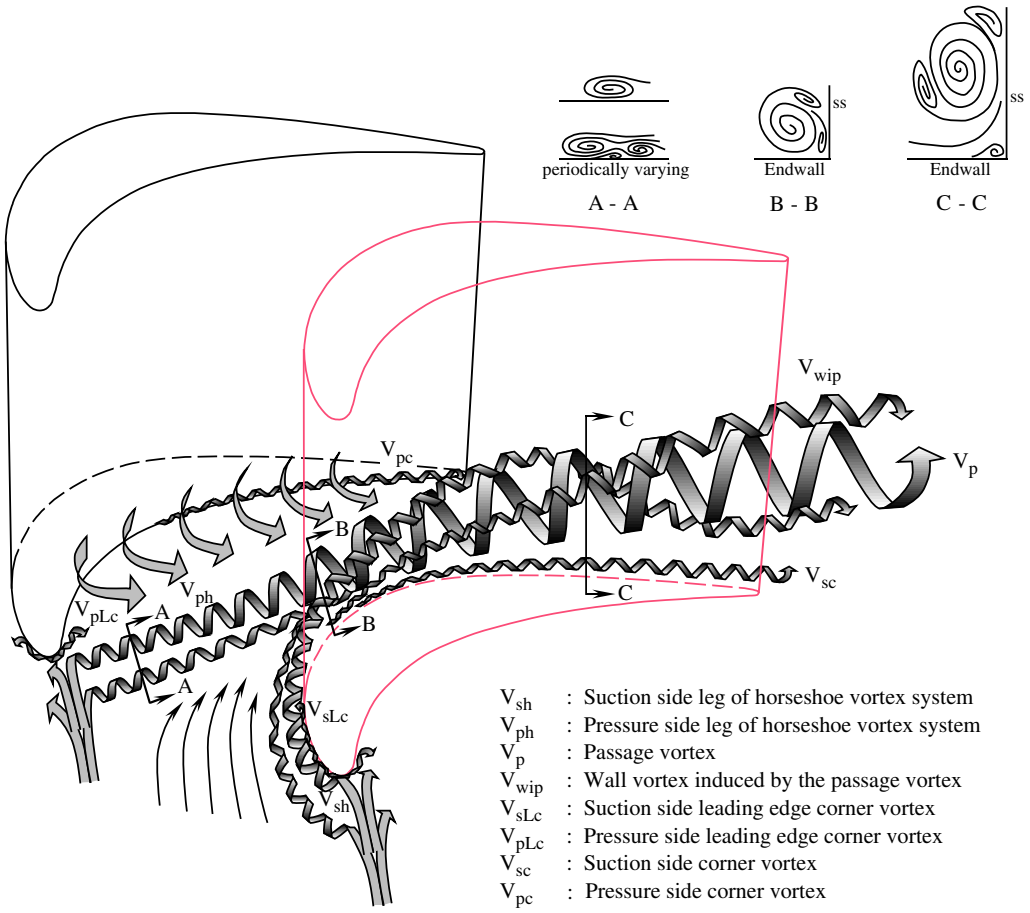

Fig. 6. Vortex model in turbine cascades from Wang et al. [19].

using commercial CFD software, to provide a constant temperature blade. It consists of a copper section, one bottom insulating section, one top insulating section, thermocouples and heaters. This blade is connected to top or middle part of the third blade in the test section. Copper is chosen, for its high conductivity, to achieve a uniform temperature on the blade surfaces. The span of the copper part is 133.3 mm and the chord is 184 mm. It has fourteen through holes for 42 cartridge heaters and one slot near the trailing edge for three strip heaters. Around the blade surfaces, 60 thermocouple holes are drilled from the top surface to the bottom surface. In these holes, thermocouples are embedded near both the pressure, suction, and tip surfaces. The positions of the thermocouples and heater holes are indicated in Figs. 7 and 8. For the insulated blades, using UHMW (ultra high molecular weight) polypropylene with a low conductivity (≈0.4 W/m K) reduces heat conduction losses. The hollow bottom insulated blade with 3 mm wall thickness and 53.97 mm height facilitates passage of heater and thermocouple wires, as well as minimizes heat conduction loss from the copper blade to the insulated blade. This heat transfer blade is fixed to the aluminum blades by screws and mounting pins. The top insulated blade is 50 mm high. For measurements in the two-dimensional regions, the top insulated blade is attached to the top of the heat transfer blade with three bolts. For three-dimensional region measurements, the top insulated section is taken out from the heat transfer blade. Then, with an additional aluminum blade, the heat transfer blade is located near the top endwall.

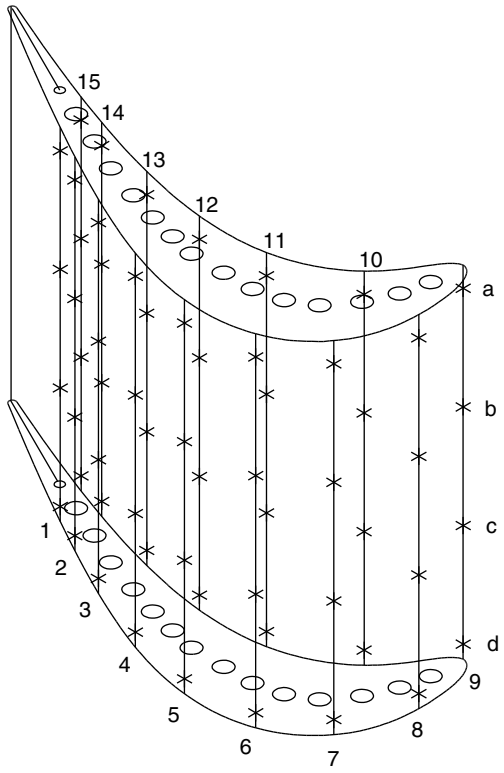

Fig. 7. Constant temperature blade with heater and thermocouple locations.

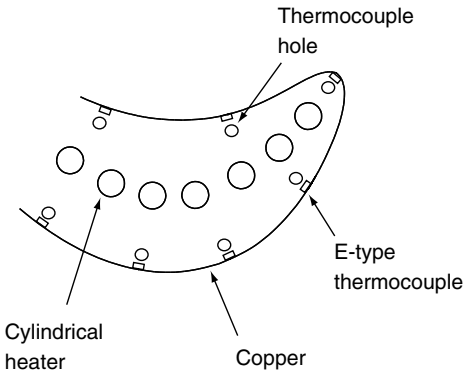

Fig. 8. Typical region of the constant temperature blade.

Heat transfer experiments with the constant temperature condition require a large number of heaters and temperature feedback in the system. Each heater needs at least one thermocouple to measure temperature and a power supply to maintain a constant temperature. The heat transfer blade in the current system has 45 heaters requiring 45 individual temperature controls. To accomplish this, a computer-controlled power supply with 128 output channels was developed at the Heat Transfer Laboratory, University of Minnesota.

3.2. Mass transfer experiment

The naphthalene sublimation technique is used to obtain local mass transfer results on the mass transfer blade. The detailed description of this technique is provided by Goldstein and Cho [5].

3.2.1. Naphthalene sublimation method

The method consists of preparing the naphthalene test section, scanning the initial surface, conducting a wind tunnel experiment, and scanning the final surface. The test surface is prepared by casting to guarantee repeatability. A constant wall concentration condition in mass transfer is equivalent to a constant wall temperature condition in heat transfer, and a non-coated surface corresponds to an adiabatic wall condition. If the surface is maintained at a uniform temperature, the naphthalene vapor pressure and concentration will be uniform. Subsequently, the boundary condition is equivalent to a constant wall temperature condition in heat transfer.

The mass diffusion coefficient of naphthalene in air (0.0681 cm^2/s) is taken to be the average of the values from Cho [13] (0.066 cm^2/s) and Chen and Wung [14] (0.0702 cm^2/s) at 298.16 K. Cho [13] states that the humidity does not significantly affect the diffusion coefficient of naphthalene in air. The saturation vapor density, $\rho_{v,w}$, is calculated from the perfect gas law equation (14)

$$\rho_{v,w} = \frac{p_{v,w}}{RT_{n,w}} = \frac{M_{naph} p_{v,w}}{\bar{R} T_{n,w}} \tag{14}$$

where $T_{n,w}$ is the surface temperature and $p_{v,w}$ is the saturation vapor pressure. The latter is obtained from a correlation by Ambrose et al. [15]. As the saturated vapor pressure is very sensitive to temperature, it is necessary to control and know the temperature of the naphthalene surface. The mass transfer coefficient is determined from

$$h_m = \frac{\dot{m}}{\rho_{v,w} - \rho_{w,\infty}} = \frac{\rho_s \delta t / \delta \tau}{\rho_{v,w}} \tag{15}$$

where $\rho_{v,w}$ is the vapor concentration at the wall and $\rho_{v,\infty} = 0$ for the mainstream.

From the mass transfer coefficient and diffusion coefficient, the Sherwood number can be expressed as

$$Sh = \frac{h_m C_l}{D_{naph}} \tag{16}$$

The uncertainty level of the Sherwood number in the naphthalene sublimation technique using the methodology described in Coleman and Steele [16] is estimated to be approximately 7% at the

95% confidence level ($\pm 2\sigma$). The measurement uncertainty not including the uncertainty of the naphthalene properties is 5.2%.

3.2.2. Mass transfer blade and measurement equipment

The mass transfer blade has the same profile as the heat transfer blade and is 197 mm in length. The mass transfer blade, made of aluminum, was used by Wang et al. [17] for two-dimensional and three-dimensional measurements without tip clearance. The mass transfer blade is shown in Fig. 9. The bottom metal cap has a tapped hole instead of a through hole and the same profile. The middle part of the test blade is about 2.5 mm deeper than the real blade. When the blade and outside mold are assembled, the gap provides space for the melted naphthalene to be cast. The cast surface has the same profile as the metal surface of the blade. The middle part of the mass transfer blade contains grooves to prevent naphthalene separation from the metal surface. The local values of sublimation depth over the naphthalene blade surface are measured with a computer-controlled four-axis data acquisition system. The whole system is essentially made from commercially-available subassemblies in Fig. 10. It moves the LVDT along the surface of the mass transfer blade and measure the sublimation depth change.

4. Results and discussion

The experiments are conducted in the two-dimensional- and three-dimensional-flow regions in the cascade. The two-dimensional-flow region experiments are conducted with each the heat or mass transfer blade in the middle of the third blade (cf. Fig. 2). The three-dimensional-flow regions experiments are conducted with the heat or mass transfer blade in the top of the third blade.

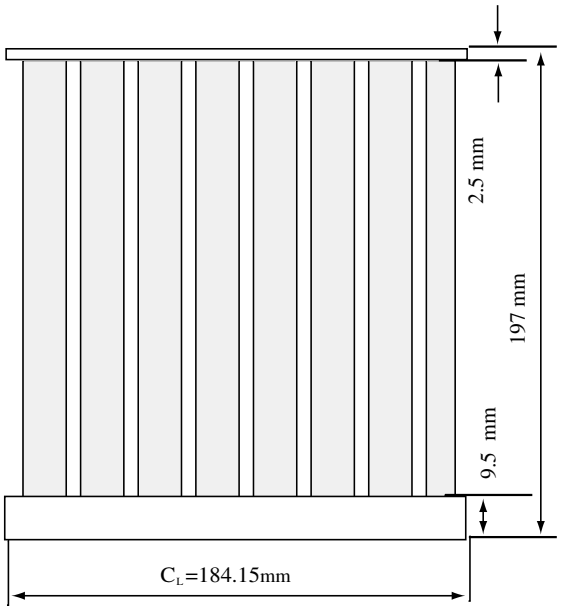

Fig. 9. Mass transfer blade.

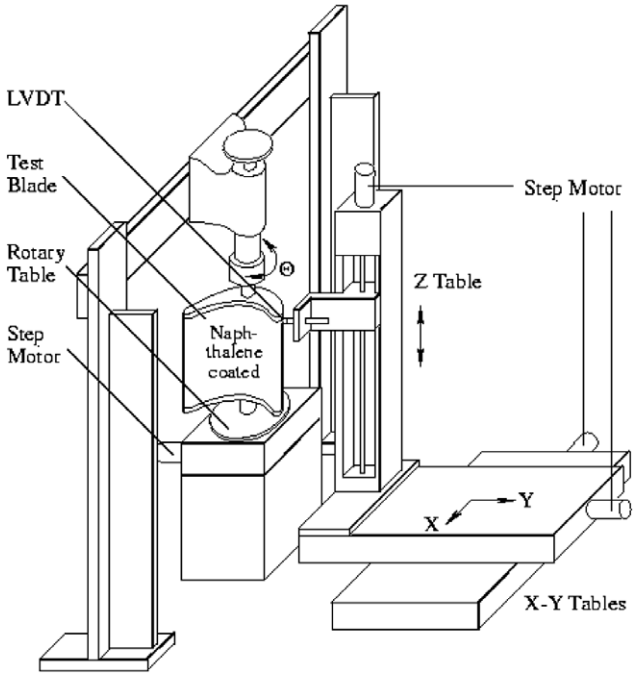

Fig. 10. Schematic of mass transfer blade measurement table.

4.1. Mass transfer measurement

In the two-dimensional case, three Reynolds numbers and two different turbulence intensities (0.2% and 12%) are used for the mass transfer experiments. Jin and Goldstein [18] measured mass transfer results in the same cascade. Their results are used to evaluate the heat and mass transfer analogy in the two-dimensional-flow region in the middle of the blade along with the present heat transfer results. Their results include tip clearance between blade and wind tunnel top. Since it is less than 1.6 mm ($t/C_l = 0.86\%$), the effect of tip clearance is negligible. The detailed experimental conditions are listed in Tables 2 and 3.

From comparison with Jin and Goldstein [18], it is confirmed that the present apparatus generates a different passage vortex because of the heat transfer measurement slot on the top endwall. The heat transfer measurement slot on the top endwall disturbs the flow near the endwall. Due to the different geometrical conditions near the top endwall, the mass transfer data from Jin and Goldstein [18] cannot be used for comparison in the three-dimensional-flow regions. Therefore, mass transfer experiments for the three-dimensional-flow regions are conducted with the present setup. One Reynolds number (2.29×10^5) and turbulence intensity ($Tu = 0.2\%$) are used to get mass transfer results for the three-dimensional-flow regions. Due to the difficulties involved with the heat transfer experiment with the high turbulence intensity near the endwall, a mass transfer experiment for comparison with a heat transfer experiment is omitted at the high turbulence intensity used. The experimental conditions are listed in Table 4.

On the suction surface, 53 measurement locations in the streamwise direction are selected. On the pressure surface, 47

Table 2
Mass transfer experimental conditions on 2D pressure surface from Jin and Goldstein [18]

No.	Run number	Location	Re_{ex}	U_{ex} (m/s)	z/C_l	Tu (%)	t/C_l (%)
1	MT-Run1-2D-P	2D-Pressure	4.79×10^5	15.5	1.5	0.2	0.86
2	MT-Run2-2D-P	2D-Pressure	5.75×10^5	18.5	1.5	0.2	0.0
3	MT-Run3-2D-P	2D-Pressure	5.33×10^5	17.2	1.5	12.0	0.86

Table 3
Mass transfer experimental conditions on 2D suction surface from Jin and Goldstein [18]

No.	Run number	Location	Re_{ex}	U_{ex} (m/s)	z/C_l	Tu (%)	t/C_l (%)
1	MT-Run1-2D-S	2D-Suction	4.44×10^5	14.4	1.5	0.2	0.86
2	MT-Run2-2D-S	2D-Suction	5.75×10^5	18.5	1.5	0.2	0.0
3	MT-Run3-2D-S	2D-Suction	5.55×10^5	17.9	1.5	12.0	0.86

Table 4
Mass transfer experiment conditions on 3D pressure and suction surfaces

Run number	Location	Re_{ex}	U_{ex} (m/s)	z/C_l	Tu (%)
MT-Run2-3D-P	3D-Pressure	2.29×10^5	19.9	0.09	0.2
				0.18	
				0.28	
MT-Run2-3D-S	3D-Suction	2.29×10^5	19.9	0.09	0.2
				0.18	
				0.28	

Table 5
Heat transfer experimental conditions on 2D pressure surface

No.	Run number	Location	Re_{ex}	U_{ex} (m/s)	z/C_l	Tu (%)
1	HT-Run1-2D-P	2D-Pressure	2.64×10^5	23.6	1.5	0.2
2	HT-Run2-2D-P	2D-Pressure	2.65×10^5	23.5	1.5	0.2
3	HT-Run3-2D-P	2D-Pressure	1.93×10^5	17.2	1.5	0.2
4	HT-Run4-2D-P	2D-Pressure	2.35×10^5	21.3	1.5	8.5
5	HT-Run5-2D-P	2D-Pressure	1.68×10^5	15.2	1.5	8.5

Table 6
Heat transfer experimental conditions on 2D suction surface

No.	Run number	Location	Re_{ex}	U_{ex} (m/s)	z/C_l	Tu (%)
1	HT-Run1-2D-S	2D-Suction	2.67×10^5	23.4	1.5	0.2
2	HT-Run2-2D-S	2D-Suction	2.43×10^5	21.7	1.5	0.2
3	HT-Run3-2D-S	2D-Suction	1.77×10^5	15.8	1.5	0.2
4	HT-Run4-2D-S	2D-Suction	2.59×10^5	23.1	1.5	8.5
5	HT-Run5-2D-S	2D-Suction	1.78×10^5	16.0	1.5	8.5

measurement locations in the streamwise direction are used. In the spanwise direction, 55 measurement locations at spanwise direction from $z/C_l = 0.01$ (near the top endwall) to 1.0 are chosen for each streamwise location. For comparison with heat transfer results, only three spanwise locations ($z/C_l = 0.09$, 0.18 and 0.28) are used in present study. Comparison with Wang et al. [17] and Jin and Goldstein [18] is provided in Fig. 11 at $z/C_l = 1$ (2D region). Since those researchers used the same test blade in the same wind tunnel, a good agreement is expected (Tables 5 and 6).

4.2. Heat transfer measurement

In the two-dimensional-flow region, the heat transfer experiments are conducted for the heat transfer blade surfaces (in Fig. 5) at spanwise position $z/C_l = 1.5$. Two Reynolds numbers and two turbulence intensities are used.

In the three-dimensional-flow region, the heat transfer coefficients are measured at three spanwise locations ($z/C_l = 0.09$, 0.18 and 0.28). The heat transfer experiments for high turbulence intensity is not conducted for the three-dimensional-flow region. The experimental conditions are presented in Tables 7 and 8.

Sample boundary layer temperature profiles are shown in Fig. 12. The data are from HT-Run3-2D-P and HT-Run3-2D-S. The wall position is zero along n-axis and monitored by the wall finding technique. In Fig. 12, temperature data below the wall position were measured and plotted when the probe moves against

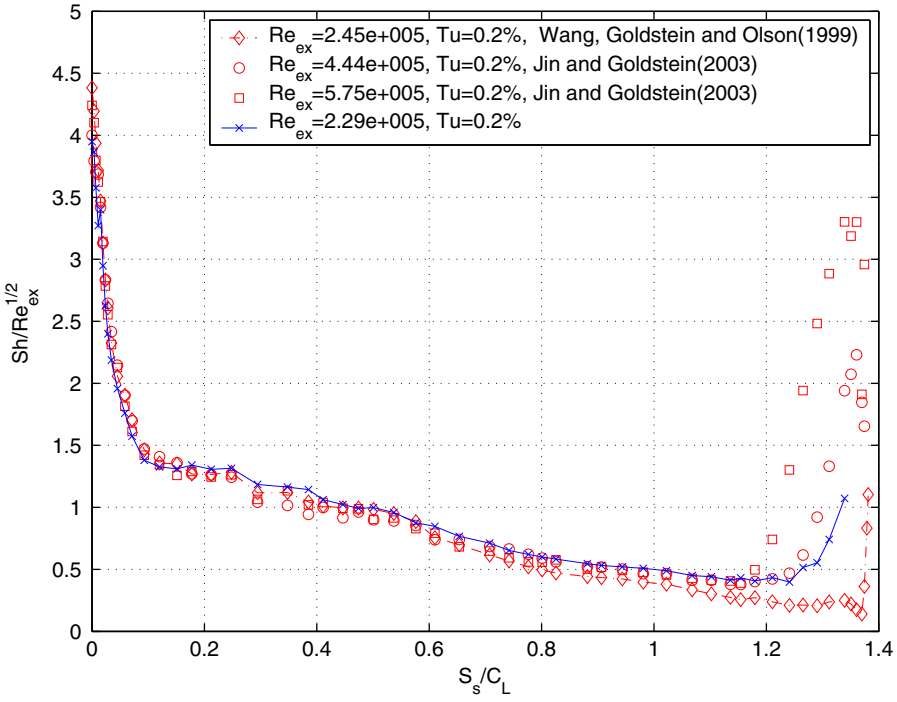

Fig. 11. Mass transfer comparison with others at $z/C_l = 1.0$ on the suction surface.

Table 7
Heat transfer experimental conditions on 3D pressure surface

No.	Run number	Location	Re_{ex}	U_{ex} (m/s)	z/C_l	Tu (%)
1	HT-Run31-3D-P	3D-Pressure	2.48×10^5	21.9	0.09	0.2
2	HT-Run32-3D-P	3D-Pressure	2.49×10^5	21.9	0.18	0.2
3	HT-Run33-3D-P	3D-Pressure	2.38×10^5	21.3	0.28	0.2

Table 8
Heat transfer experimental conditions on 3D suction surface

No.	Run number	Location	Re_{ex}	U_{ex} (m/s)	z/C_l	Tu (%)
1	HT-Run31-3D-S	3D-Suction	2.41×10^5	21.4	0.09	0.2
2	HT-Run32-3D-S	3D-Suction	2.41×10^5	21.4	0.18	0.2
3	HT-Run33-3D-S	3D-Suction	2.41×10^5	21.4	0.28	0.2

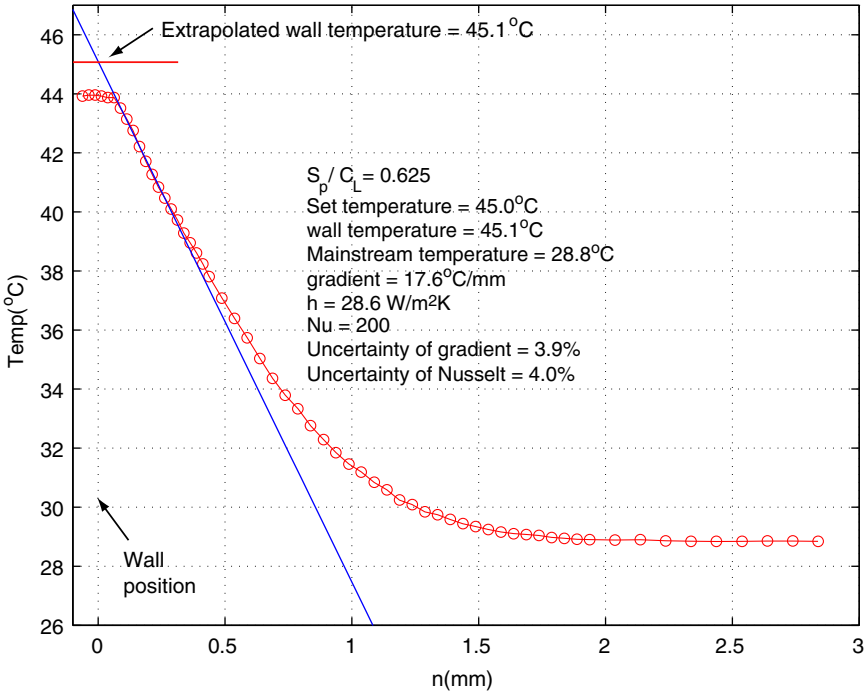

(a) pressure surface

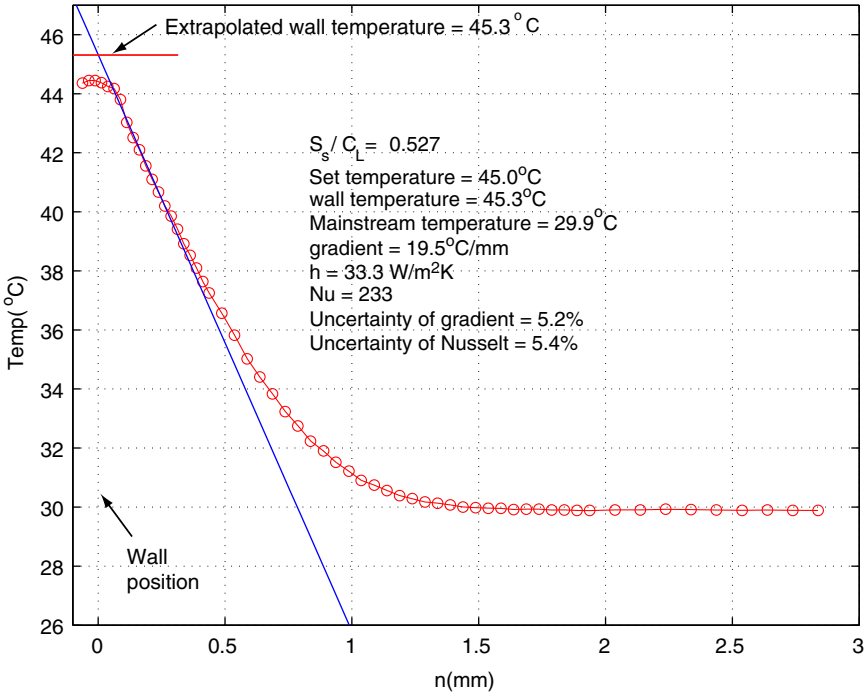

(b) suction surface

Fig. 12. Sample thermal boundary layer profile on the blade.

the wall to make sure a contact between the probe and the wall. The linear conduction region near the wall is used to calculate a heat flux from the wall. The wall temperature is found from extrapolation of the temperature profile in the linear region. The wall temperature is the intersection between the least square fit line and the wall position. The wall position is known from the motion controller program with a precision of ±2.5 μm. Therefore, if the wall temperature is properly controlled and the wall position is accurately found, the extrapolated wall temperature should be close to the set temperature. However, the extrapolated wall temperature (45.1 °C and 45.3 °C) is more than the set temperature (45.0 °C) by 0.1 °C and 0.3 °C due to the small number of heaters and thermocouples in the blade at the location examined in Fig. 12.

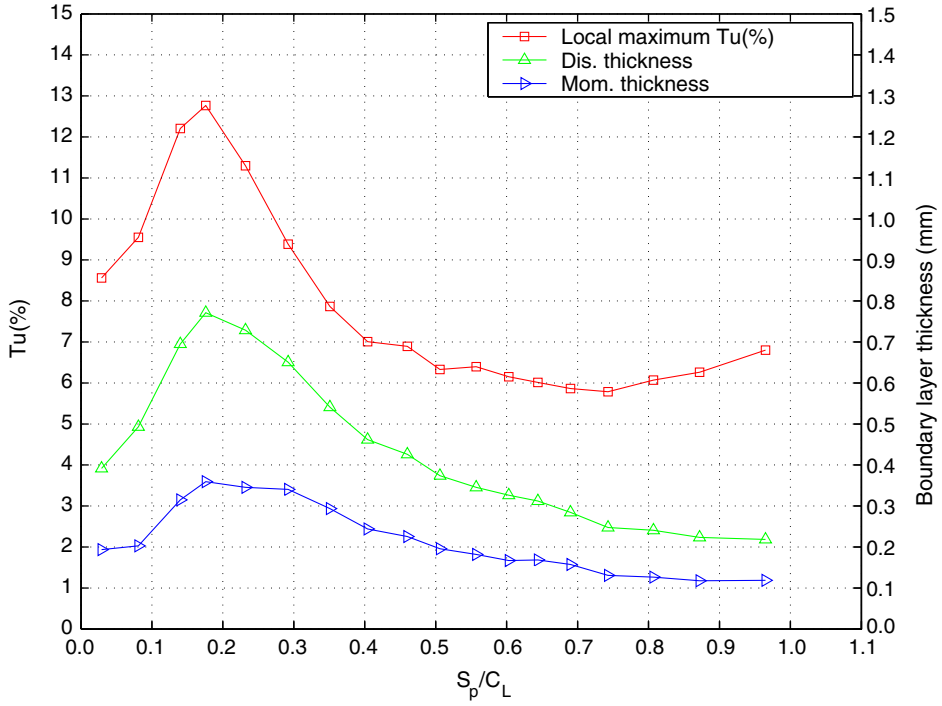

(a) pressure surface

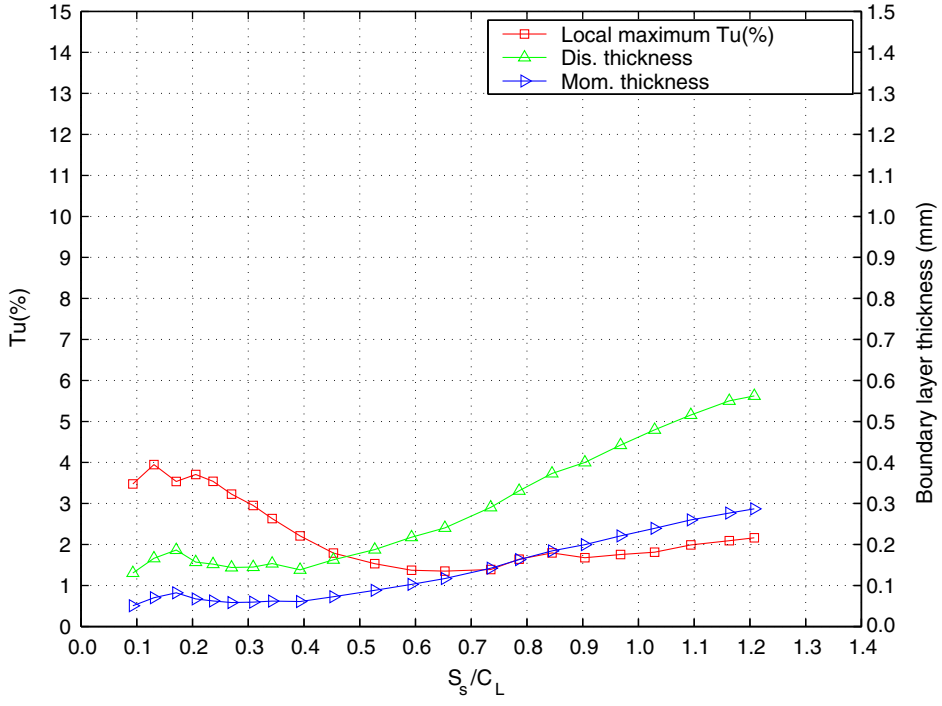

(b) suction surface

Fig. 13. Boundary layer thickness and turbulence intensity at $Re_{ex} = 1.9 \times 10^5$ and $z/C_l = 1.0$.

The heat transfer results are measured from $S_s/C_l = 0.074$ (suction surface) to the trailing edge. Due to the access limitation, this is the closest position to the leading edge that can be achieved on the suction surface. For the pressure surface, measurement are taken from the leading edge ($S_p/C_l = 0.0$) to the trailing edge. The heat transfer data are acquired at low Reynolds number flow and do not show early transition on the suction side in the two-dimensional regions even at high turbulence intensity. The heat transfer measurements are limited in the high heat transfer regions. Very thin thermal boundary layers result in significant errors and high uncertainty.

4.3. Heat and mass transfer analogy

For the two- and three-dimensional-flow regions, Nusselt and Sherwood numbers are compared to examine the validity of the heat/mass transfer analogy on a turbine blade. The Nusselt and Schmidt numbers are expressed in Eq. (4). To ease comparison,

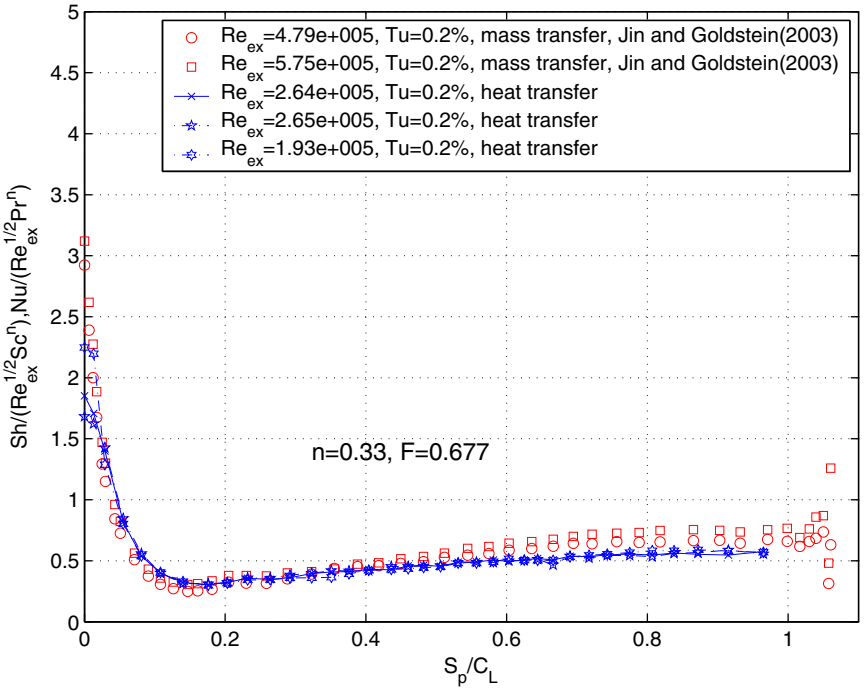

Fig. 14. Heat/mass analogy with $n = 1/3$ at $z/C_l = 1.5$ (2D-flow) on the pressure surface.

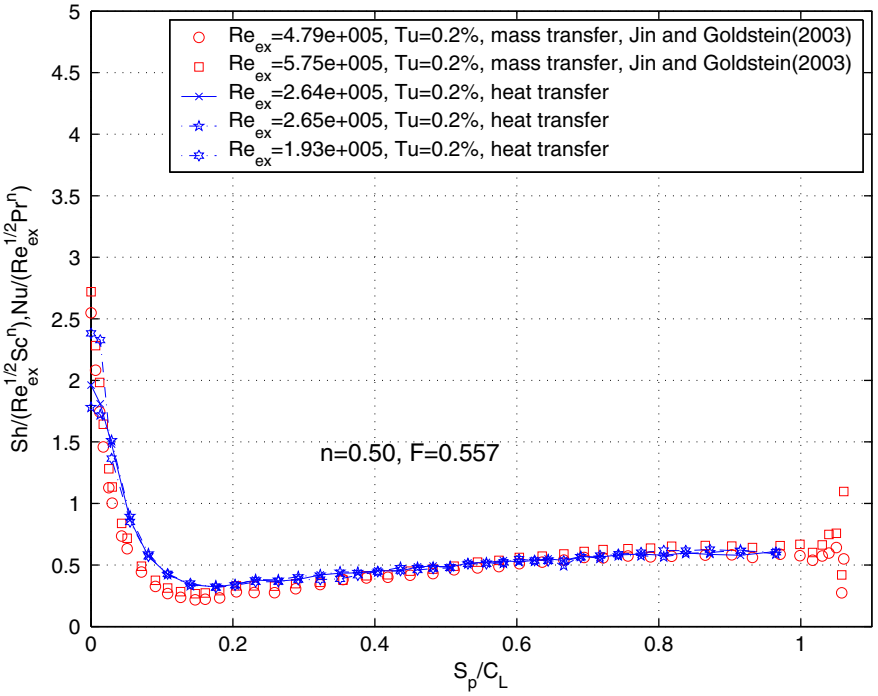

Fig. 15. Heat/mass analogy with $n = 0.5$ at $z/C_l = 1.5$ (2D-flow) on the pressure surface.

the Nusselt number is normalized, $Nu/(Re_x^{1/2}Pr^n)$ with $Pr = 0.707$ (air), as is the Sherwood number, $Sh/(Re_x^{1/2}Sc^n)$ with $Sc = 2.28$ (naphthalene). Two different values of 'n' are traced – '$n = 1/3$' ($F = 0.677$) for the laminar flow and '$n = 0.5$' ($F = 0.557$) for the turbulence flow.

Flow over the blade is not tripped by a wire or other intentional roughness. More or less naturally, the boundary layer on the blade changes from laminar to turbulent. Careful attention should be given to the development of the flow on both pressure and suction surfaces. Local maximum turbulence intensity,and momentum and displacement thicknesses at $z/C_l = 1.0$ (two-dimensional region), $Re = 1.9 \times 10^5$ and $Tu = 0.2\%$ in free stream are plotted in Fig. 13 for the pressure and suction sides, to show the flow development. To measure them, the five-axis system and a single hot-wire probe are used instead of the thermal boundary layer probe. On the same location of the heat transfer measurement for both

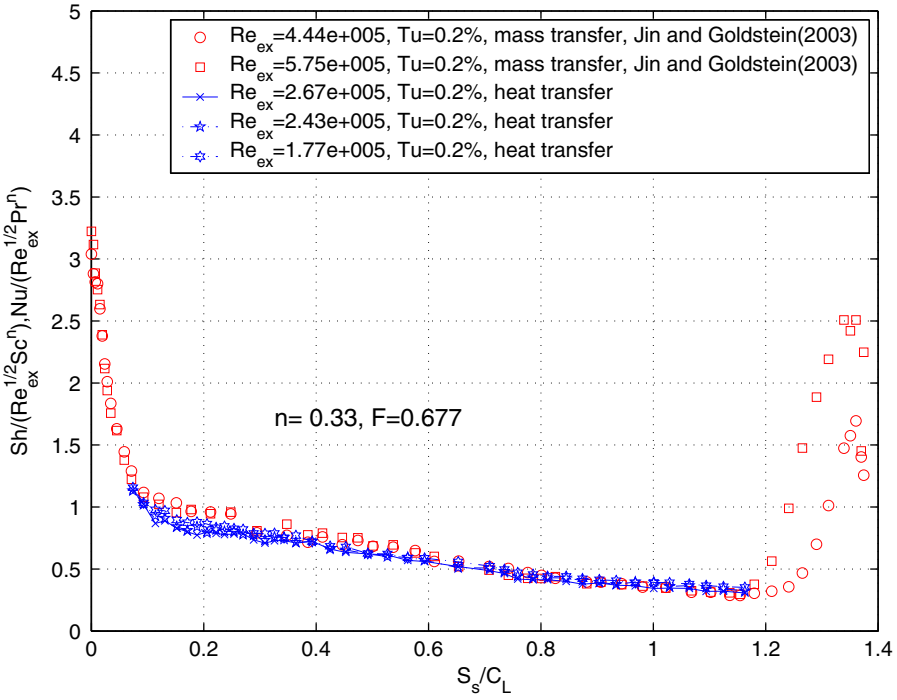

Fig. 16. Heat/mass analogy with $n = 1/3$ at $z/C_l = 1.5$ (2D-flow) on the suction surface.

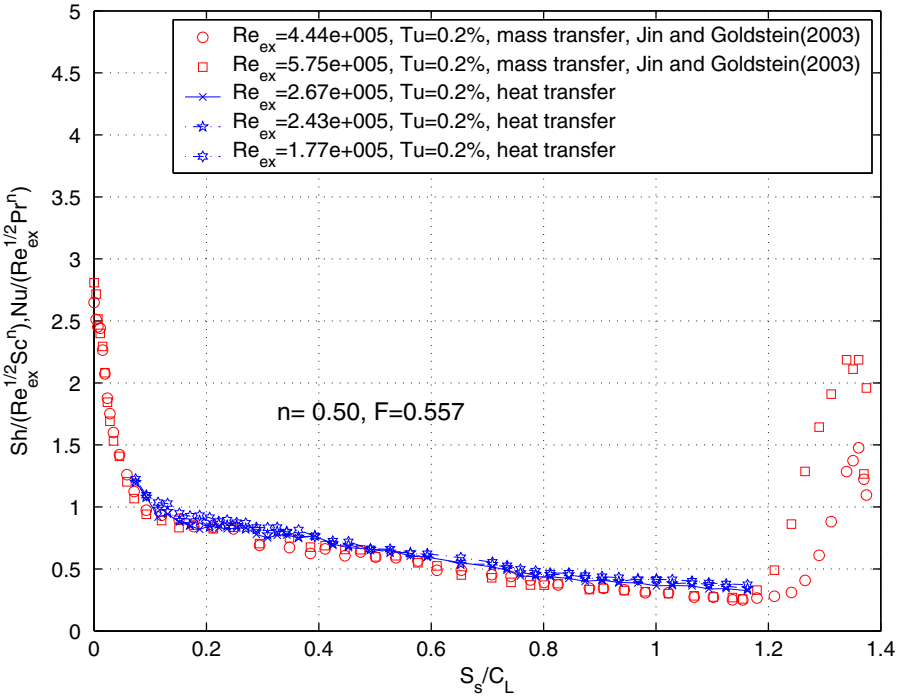

Fig. 17. Heat/mass analogy with $n = 0.5$ at $z/C_l = 1.5$ (2D-flow) on the suction surface.

pressure and suction surface, flow velocities are measured when the hot-wire moves out from the blade surface. The momentum and displacement thicknesses on the pressure surface increase with S near the leading edge and then decrease due to strong flow acceleration. The local maximum turbulence intensity near the wall increases up to $S_p/C_l = 0.2$ and then decreases on the downstream part of the pressure side. Even though the boundary layer appears to experience relaminarization, it has a high local turbulence intensity (>6%) on the entire pressure surface. On the suction surface, the momentum and displacement thicknesses reach small minima near the leading edge and then grow again from $S_s/C_l = 0.4$. The local maximum turbulence intensity decreases from 4% to 1.2% at $S_s/C_l = 0.6$ and then increments further downstream.

4.3.1. Two-dimensional-flow region

Heat and mass transfer comparisons for '$n = 1/3$' ($F = 0.677$) and '$n = 0.5$' ($F = 0.557$) are shown in Figs. 14 and 15 for the pressure

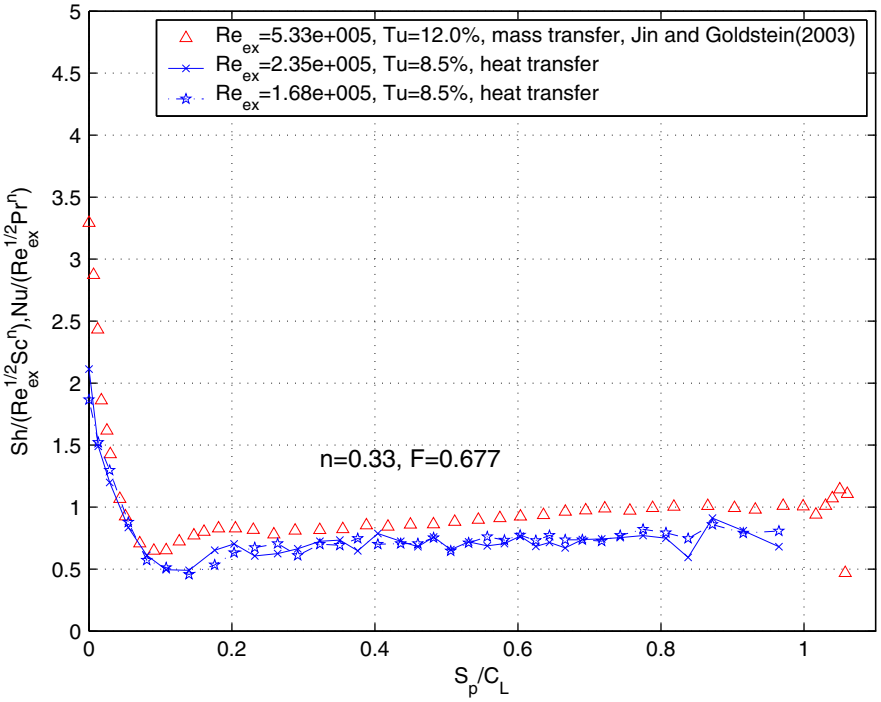

Fig. 18. Heat/mass analogy with $n = 1/3$ at $z/C_l = 1.5$ (2D-flow) on the pressure surface and $Tu = 8.5\%$.

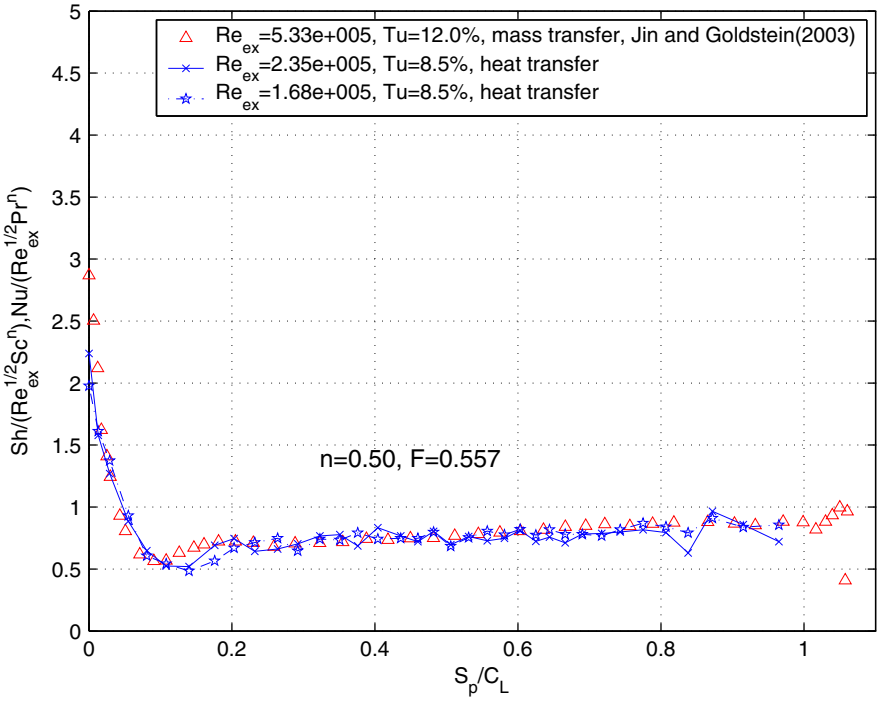

Fig. 19. Heat/mass analogy with $n = 0.5$ at $z/C_l = 1.5$ (2D-flow) on the pressure surface and $Tu = 8.5\%$.

surface in the two-dimensional-flow region. Due to the boundary layer development from laminar to turbulent, '$n = 1/3$' ($F = 0.677$) shows a good agreement near the leading edge, up $S_p/C_l = 0.2$, and '$n = 0.5$' ($F = 0.557$) shows a good agreement on the downstream part of the blade. Strictly speaking, the analogy factor, F is not constant on the blade surface. As expected, the development of the boundary layer from laminar to turbulent alters the analogy factor. The Nusselt number from the leading edge to $S_p/C_l = 0.05$ is smaller than Sherwood number with the analogy factor (0.557 or 0.677) in Figs. 14 and 15. One of the possible reasons is the limitation of heat transfer measurement. Near the leading edge, the flow has a very thin thermal boundary layer. Therefore, the results are affected by the conduction error in the probe. It is difficult to measure temperature properly if the thickness of the linear region is

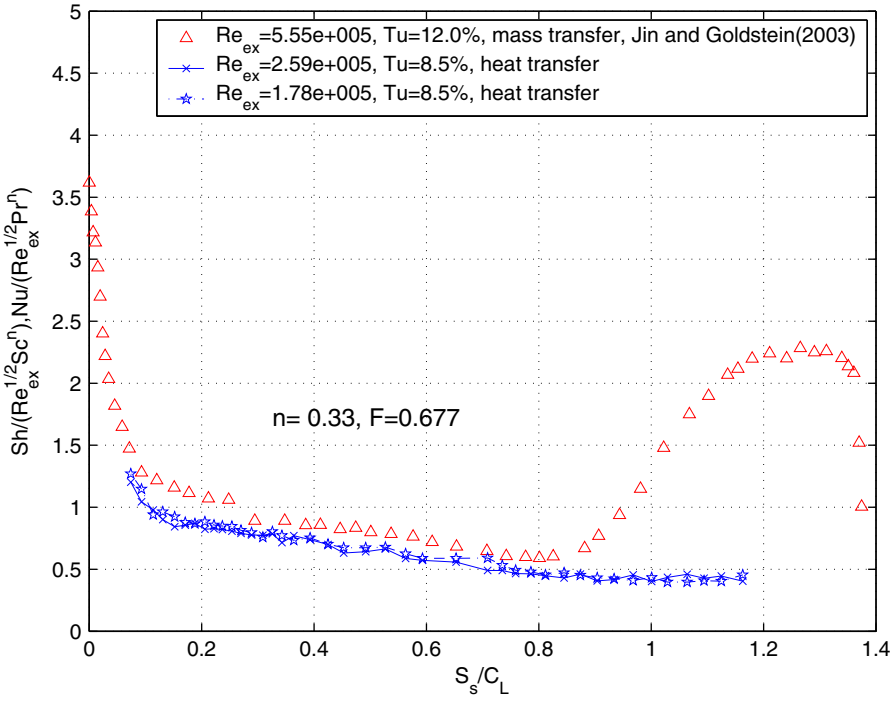

Fig. 20. Heat/mass analogy with $n = 1/3$ at $z/C_l = 1.5$ (2D-flow) on the suction surface and $Tu = 8.5\%$.

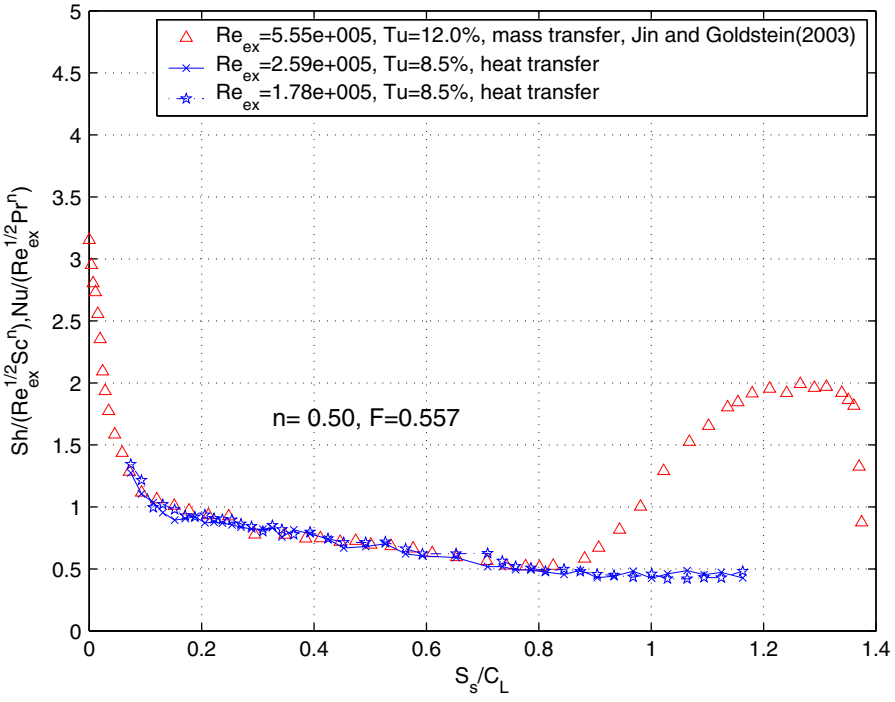

Fig. 21. Heat/mass analogy with $n = 0.5$ at $z/C_l = 1.5$ (2D-flow) on the suction surface and $Tu = 8.5\%$.

less than 100 μm. In addition, near the stagnation line small misalignment of the probe can have big impact to compare the heat and mass transfer results.

Figs. 16 and 17 provide heat and mass transfer comparisons with '$n = 1/3$' and '$n = 0.5$' on the suction surface in the two-dimensional-flow region. Due to the limitation of the measurement slot, comparisons are made only from $S_s/C_l = 0.074$ to $S_s/C_l = 1.2$. Using '$n = 1/3$' ($F = 0.677$) provides a good match for $S_s/C_l > 0.65$ to the transitional region ($S_s \approx 1.2$) in Fig. 16. Using '$n = 0.5$' ($F = 0.557$) provides a good agreement from $S_s/C_l = 0.074$ to $S_s/C_l = 0.65$ in Fig. 17. The value of the analogy factor on the suction surface is affected by variation in the local maximum turbulence intensity and boundary layer development as indicated in Fig. 13. Thus, '$n = 1/3$' ($F = 0.677$) in Fig. 16 shows a good agreement in lower local turbulence intensity region and thicker boundary layer region, Fig. 13b and '$n = 0.5$' ($F = 0.557$) in Fig. 17 shows a

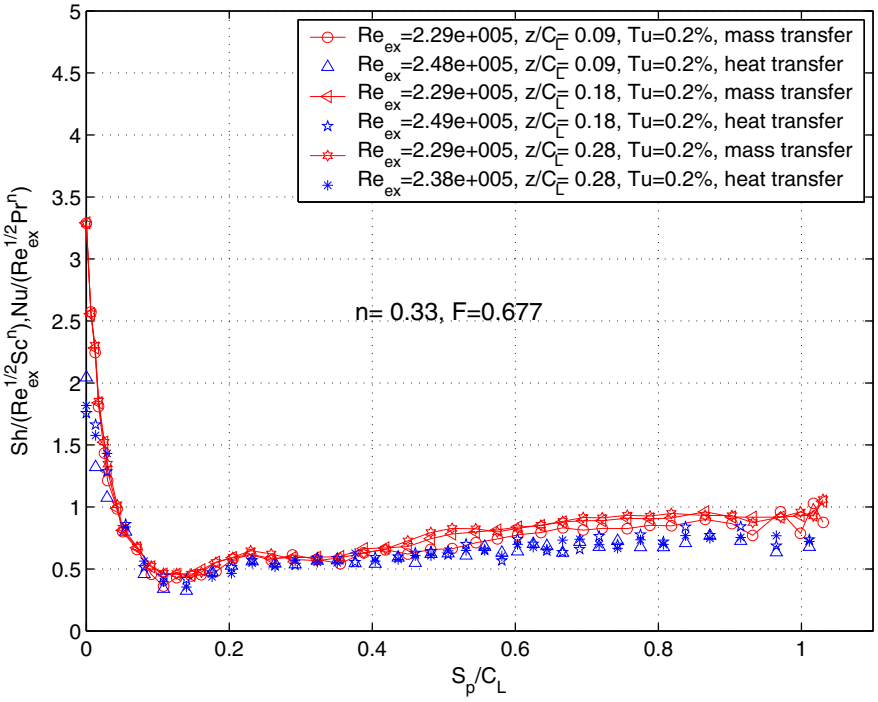

Fig. 22. Heat/mass analogy with $n = 1/3$ on the pressure side in three-dimensional region.

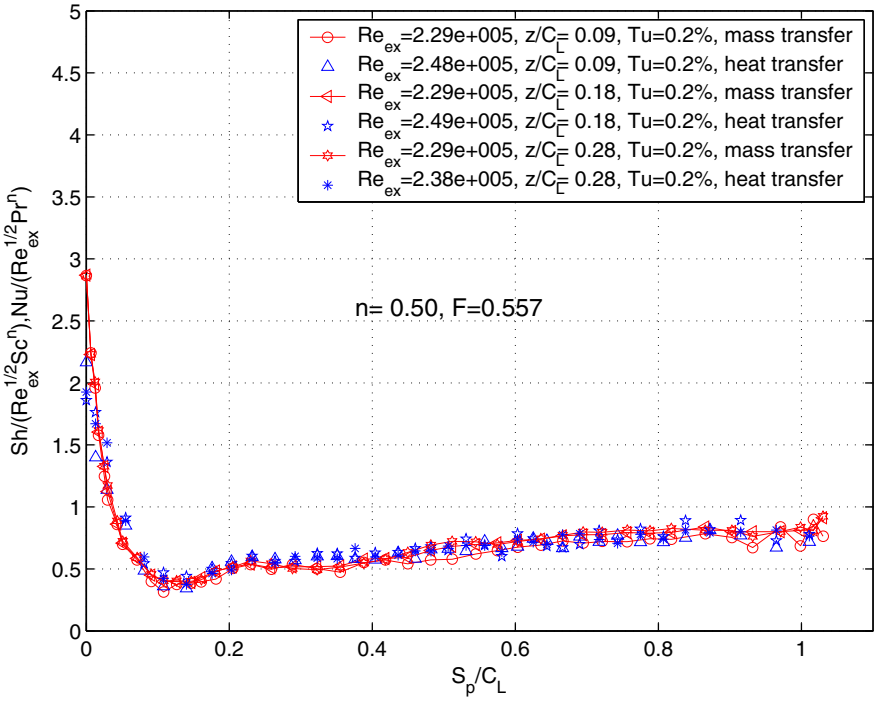

Fig. 23. Heat/mass analogy with $n = 0.5$ on the pressure side in three-dimensional region.

good agreement in higher local turbulence intensity regions and thinner boundary layer regions, Fig. 13b.

A high turbulence intensity, $Tu = 8.5\%$, is used for heat transfer measurement while $Tu = 12\%$ was used in the mass transfer measurements of Jin and Goldstein [18]. Figs. 18 and 19 compare the heat/mass transfer analogy on the pressure side for high free stream turbulence. Fig. 19 shows that the analogy factor does not change from $S_p/C_l = 0.2$ to $S_p/C_l = 1.0$ on the pressure surface with the high free stream turbulence. A constant value, '$n = 0.5$' ($F = 0.557$) on the pressure surface appears valid with high turbulence intensity. The high turbulence intensity apparently develops the flow on the pressure surface faster at the lower turbulence intensity.

Figs. 20 and 21 compare the heat and mass transfer results on the suction side for high turbulence intensity. The mass transfer results in Fig. 21 indicate early transition ($S_s/C_l \approx 0.85$), but the heat

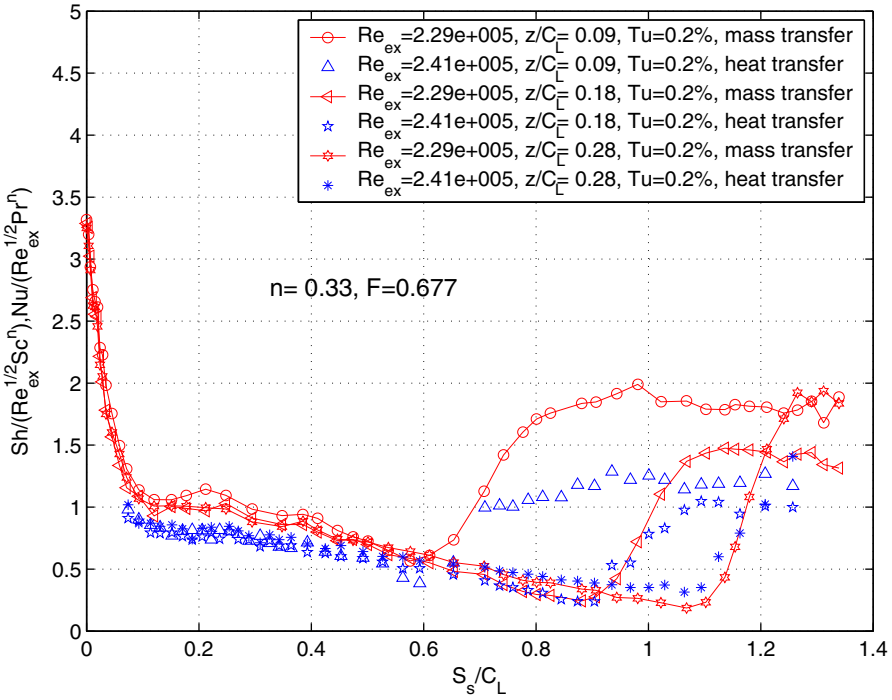

Fig. 24. Heat/mass analogy with $n = 1/3$ on the suction side in three-dimensional region.

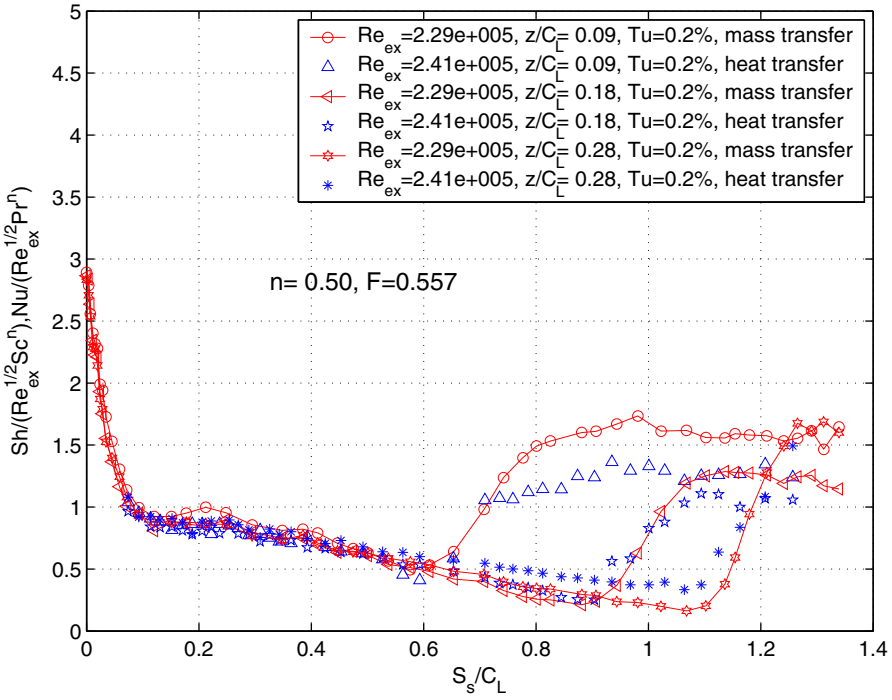

Fig. 25. Heat/mass analogy with $n = 0.5$ on the suction side in three-dimensional region.

transfer results do not, probably because the latter are obtained at low Reynolds number. At the high turbulence intensity, the analogy factor has a constant value ($n = 0.5$, $F = 0.557$) from $S_s/C_l = 0.074$ to $S_s/C_l \approx 0.85$. At large S_s/C_l, the flow experiences early transition in the higher Reynolds number mass transfer experiment. Turbulence weaken relaminarization of the flow and induce fully-developed turbulence flow on the suction side.

4.3.2. Three-dimensional-flow region

Figs. 22–25 compare heat and mass transfer results at $z/C_l = 0.09$, $z/C_l = 0.18$ and $z/C_l = 0.28$ in the three-dimensional-flow regions. The three-dimensional-flow regions are generated by the passage vortex near the endwall. This primarily affects the heat/mass transfer on the suction surface. Figs. 22 and 23 show that on the pressure surface, '$n = 1/3$' and '$n = 0.5$' match the heat transfer results with mass transfer results at different value of Z. This value, '$n = 0.5$' ($F = 0.557$), is valid along the pressure side except the leading edge at all spanwise positions. Near the leading edge, '$n = 1/3$' matches the heat and mass transfer results well as in the two-dimensional-flow regions. Note the current heat transfer results near the stagnation line suffer inaccuracy due to the conduction error and the difficulty of the probe alignment.

On the suction side, '$n = 0.5$' ($F = 0.557$) matches heat transfer results to mass transfer results near the endwall before the passage vortex touches the surface in Figs. 24 and 25. At large spanwise positions (z/C_l), the touch point of the passage vortex moves downstream which is clearly shown. At the triangular region caused by the passage vortex, heat and mass transfer results do not show a good agreement with '$n = 0.5$' ($F = 0.557$). There are complex flows in this region including vortices, reverse flow, separation and etc. Note the heat transfer results are not properly evaluated in this region where '$n = 0.6$' ($F = 0.495$) and '$n = 0.7$' ($F = 0.441$) can be used to match heat and mass transfer results. However, the exact analogy factors are still questionable in these regions where vortices impinge or separate on the surface as the heat transfer measurements are more uncertain there.

5. Conclusions

Heat and mass transfer experiments with equivalent boundary conditions have been conducted to investigate the heat/mass transfer analogy on a blade in a simulated turbine cascade. The heat transfer and mass transfer data are compared with $Nu/(Re_x^{1/2}Pr^n)$ with $Pr = 0.707$ and $Sh/(Re_x^{1/2}Sc^n)$ with $Sc = 2.28$, respectively.

Heat transfer measurements in the two-dimensional-flow region on the blade have been compared with mass transfer data from Jin and Goldstein [18]. A value '$n = 1/3$' ($F = 0.677$) works well in the laminar regions, while '$n = 0.5$' ($F = 0.557$) appears best for the turbulent regions. With low turbulence intensity, the analogy factor appears to change along the development of the flow on both pressure and suction surfaces. However, the analogy factor seems to be a constant value for both pressure and suction surfaces with high turbulence intensity.

Heat and mass transfer measurements conducted on the blade near the endwall also indicate '$n = 1/3$' ($F = 0.677$) for laminar regions and '$n = 0.5$' ($F = 0.557$) for turbulent regions in the three-dimensional-flow region. Near the wall, the analogy factor on both pressure and suction surfaces are similar to the value in a two-dimensional-flow region with high free stream turbulence. Near the endwall, '$n = 0.5$' ($F = 0.557$) is valid for the pressure and suction surfaces except the triangular region on the suction side, affected strongly by the passage vortex in the triangular region. In this region, '$n = 0.6$' ($F = 0.495$) or '$n = 0.7$' ($F = 0.441$) can be used to match heat and mass transfer coefficients. However, the exact analogy factor is still questionable where the complicated secondary flows occur. Errors in the heat transfer measurements near the leading edge also can cause significant uncertainty in the analogy factors.

Acknowledgements

The authors would like to acknowledge DOE for support. Thank the financial support (02-01-SR096), University Turbine System Research Program.

References

[1] W. Nusselt, Wärmeübergang, diffusion und verdunstung, Math. Mech. 2 (1930) 105–121.
[2] E. Schmidt, Verdunstung und wärmeügergang, Gesund. Ing. 29 (1929) 525–529.
[3] J.S. Lewis, A heat/mass transfer analogy applied to fully developed turbulent flow in an annulus, J. Mech. Eng. Sci. 13 (4) (1971) 286–292.
[4] P.H. Chen, R.J. Goldstein, Convective transport phenomena on the suction surface of a turbine blade including the influence of secondary flows near the endwall, J. Turbomach. 114 (1992) 776–787.
[5] R.J. Goldstein, H.H. Cho, A review of mass transfer measurements using naphthalene sublimation, Exp. Thermal Fluid Sci. 10 (1995) 416–434.
[6] E.R.G. Eckert, H. Sakamoto, T.W. Simon, The heat/mass transfer analogy factor, nu/sh, for boundary layers on turbine blade profiles, Int. J. Heat Mass Transfer 44 (2001) 1223–1233.
[7] S.-Y. Yoo, J.-H. Park, C.-H. Chung, M.-K. Chung, An experimental study on heat/mass transfer from a rectangular cylinder, J. Heat Transfer 125 (2003) 1163–1169.
[8] S. Han, R. Goldstein, The heat/mass transfer analogy for a simulated turbine endwall, Int. J. Heat Mass Transfer 51 (11–12) (2008) 3227–3244.
[9] E.R.G. Eckert, R.M. Drake, Analysis of Heat and Mass Transfer, McGraw-Hill, New York, 1972.
[10] W.M. Kays, M.E. Crawford, Convective Heat and Mass Transfer, third ed., McGraw-Hill, New York, 1993.
[11] S. Han, R. Goldstein, Heat transfer study in a linear turbine cascade using a thermal boundary layer measurement technique, ASME J. Heat Transfer 129 (10) (2007) 1384–1394.
[12] B.F. Blackwell, R.J. Moffat, Design and construction of a low velocity boundary temperature probe, J. Heat Transfer 97 (2) (1975) 313–315.
[13] K. Cho, Measurement of the diffusion coefficient of naphthalene into air, Ph.D. Thesis, State Univ. New York at Stony Brook, 1989.
[14] P.H. Chen, P.H. Wung, Diffusion coefficient of naphthalene in air at room temperature, personal communication.
[15] D. Ambrose, I. Lawrenson, C. Sparke, The vapor pressure of naphthalene, J. Chem. Thermodyn. 7 (1975) 1173–1176.
[16] H.W. Coleman, W.G. Steele, Experimentation and Uncertainty Analysis for Engineers, second ed., A Wiley-Interscience Publication, 1999.
[17] H.P. Wang, R.J. Goldstein, S.J. Olson, Effect of high free-stream turbulence with large length scale on blade heat mass transfer, J. Turbomach. 121 (1999) 217–224.
[18] P. Jin, R.J. Goldstein, Local mass/heat transfer on turbine blade near-tip surfaces, J. Turbomach. 125 (3) (2003) 521–528.
[19] H.P. Wang, S.J. Olson, R.J. Goldstein, E.R.G. Eckert, Flow visualization in a linear turbine cascade of high performance turbine blades, ASME J. Turbomach. 119 (1997) 1–8.